Journal of Environmental Management 391 (2025) 126501

Contents lists available at ScienceDirect

Journal of Environmental Management

journal homepage: www.elsevier.com/locate/jenvman

Research article

Use of biochar and coal ash as passive sorbent barriers for long-term mitigation of chlorinated solvent vapours

Clarissa Settimi [a], Benedetta Conti [a], Iason Verginelli [a,*], Daniela Zingaretti [a], Immacolata Bortone [b], Frederic Coulon [b], Renato Baciocchi [a]

[a] Department of Civil Engineering and Computer Science Engineering, University of Rome Tor Vergata, Via del Politecnico 1, 00133, Rome, Italy
[b] Cranfield University, Faculty of Engineering and Applied Sciences, Cranfield, MK43 0AL, UK

ARTICLE INFO

Keywords:
Biochar
Chlorinated VOCs
Adsorption
Contaminated sites
Risk management strategies

ABSTRACT

This study explores the potential of biochar and coal ashes as novel passive sorbent barriers to mitigate chlorinated solvent vapours at contaminated sites, addressing the need for sustainable risk mitigation alternatives to traditional remediation. Trichloroethylene (TCE) was used as a model compound in adsorption batch tests under varying temperatures (5–35 °C) and humidity levels (0–50 %) to evaluate the adsorption capacity of biochar derived from pyrolysed biomass and coal ash from wood pellets gasification. All materials exhibited good adsorption capacities (75–170 mg g^{-1}), with biochar outperforming coal ashes due to higher carbon content. Adsorption capacity showed a decline with increasing temperature and humidity of maximum 30 %, consistent with exothermic physical adsorption. Freundlich isotherms best described the adsorption behaviour, suggesting a non-linear, reversible, and multilayer process. Column adsorption tests of TCE vapours were then carried out with biochar to assess the adsorption behaviour under dynamic conditions showing good performance. Modelling revealed that a 50 cm thick barrier of biochar could effectively mitigate chlorinated vapours for over 15 years for entering concentrations up to 1 g m^{-3}, proving the suitability of the tested materials as long-term risk management solutions in the subsurface. The overall results challenge the prevailing reliance on traditional remediation systems, highlighting the potential of a passive risk mitigation approach aligned with sustainability objectives and advancing knowledge in this field.

1. Introduction

Carbonaceous materials have been widely recognised for their effectiveness in adsorbing contaminants from soil and water (Ahmad et al., 2014; Qiu et al., 2022; Zhu et al., 2020). Among them, activated carbon (AC) is the most commonly used material, primarily due to its significant adsorption capacity, which is attributed to the high porosity developed during its production via chemical or thermal activation of coal (Ahmad et al., 2014; Yuan et al., 2019; Rossi et al., 2021). However, the reliance on virgin materials needed for AC production has driven interest in more sustainable alternatives, particularly carbonaceous materials derived from the thermal treatment of waste biomass (Qiu et al., 2022; Balsamo et al., 2013). Among these materials, biochar (BC), obtained through the pyrolysis of biomass under limited or no oxygen conditions, has emerged as a promising low-cost alternative to AC (Ahmad et al., 2014; Yuan et al., 2019; Kumar and Bhattacharya, 2021). Studies have highlighted the benefits of using biochar from waste biomass, including lower costs and improved environmental sustainability compared to conventional AC. (Alhashimi and Aktas, 2017; Kamali et al., 2021). BC is characterised by a porous structure and can be produced at relatively low temperatures without the need for additional activation. It can be obtained from a wide range of feedstocks, including crop residues (e.g., husks, shells, straw, manure), forestry by-products (e.g., wood), food waste, and sewage sludge (Ahmad et al., 2014; Kumar and Bhattacharya, 2021; Li et al., 2021b; Lu et al., 2025; An et al., 2024). Similarly, coal ashes from biomass gasification processes have shown potential as low-cost alternative adsorbents (Zhu et al., 2020; Balsamo et al., 2013; Galhetas et al., 2014; Benedetti et al., 2018; Ribeiro et al., 2019), offering the additional advantage of promoting resource recovery and reducing waste disposal (Ribeiro et al., 2019).

Although waste-derived carbonaceous materials have been extensively investigated for the adsorption of a wide range of contaminants,

* Corresponding author.
E-mail addresses: settimi@ing.uniroma2.it (C. Settimi), benedetta.conti@alumni.uniroma2.eu (B. Conti), verginelli@ing.uniroma2.it (I. Verginelli), zingaretti@ing.uniroma2.it (D. Zingaretti), imma.bortone@cranfield.ac.uk (I. Bortone), f.coulon@cranfield.ac.uk (F. Coulon), baciocchi@ing.uniroma2.it (R. Baciocchi).

https://doi.org/10.1016/j.jenvman.2025.126501
Received 13 January 2025; Received in revised form 12 June 2025; Accepted 6 July 2025
Available online 11 July 2025

including metals, organic pollutants, emerging contaminants and volatile organic compounds (VOCs) (Da Silva Santos et al., 2021; Huang et al., 2023; Kaikiti et al., 2021; Lyu et al., 2023; Qiu et al., 2022; Sadegh et al., 2024; Shen, 2023; Zhang et al., 2017a, 2017b; Zhao et al., 2022), their application for halogenated VOCs (HVOCs), and particularly chlorinated VOCs (CVOCs), remains relatively underexplored (Hsu et al., 2014; Klasson et al., 2009; Kumar et al., 2020; Makoś-Chełstowska et al., 2024; Nikam and Mandal, 2020; Xiang et al., 2020). CVOCs such as trichloroethylene (TCE), are widespread environmental pollutants due to their historical use in industrial and commercial processes (Damgaard et al., 2013; Hsu et al., 2014; Pochampally et al., 2023). These compounds pose considerable challenges in contamination management because of their low biodegradability and dense non-aqueous phase liquid (DNAPL) behaviour, enabling deep subsurface migration and creating persistent and diffuse contamination sources (U.S. EPA, 2004). Furthermore, chlorinated solvents can volatilise from subsurface sources, leading to vapour intrusion into indoor air and posing significant health risks (Ma et al., 2020).

In scenarios of diffuse contamination by CVOCs, traditional remediation techniques are often technically and economically unsustainable, highlighting the need for cost-effective risk management alternatives. In this context, recent studies have proposed the passive treatment of contaminated vapours in the vadose zone using reactive materials such as potassium permanganate, zero-valent iron (ZVI), or ZVI-based bimetals incorporated into horizontal permeable reactive barriers (HPRBs) (Mahmoodlu et al., 2015; Settimi et al., 2023, 2025; Zingaretti et al., 2020). Similarly, sorbent materials could be used in passive sorbent barriers (i.e., horizontal permeable adsorbing barriers, HPABs) for CVOCs vapour remediation and associated risk mitigation. Although sorbent-based barriers have been employed in other contexts, such as biocovers for landfill gas management (Chavan and Kumar, 2018; Scheutz and Kjeldsen, 2003) or capping (Wang et al., 2024), the use of HPABs at contaminated sites specifically targeting chlorinated vapours remains unexplored. Carbonaceous materials such as biochar and coal ashes, which have shown potential as low-cost and sustainable adsorbents for VOCs (Ribeiro et al., 2019; Sadegh et al., 2024; Zhao et al., 2022), have not yet been investigated for their efficacy in HPAB systems targeting chlorinated vapours.

Therefore, this study aims to investigate the potential of various biochars and coal ashes for CVOCs adsorption, using TCE as a model compound, and to assess their suitability as functional components of HPABs. These objectives were addressed by performing TCE vapours adsorption tests in batch and column systems at laboratory scale, coupled with modelling simulations aimed at evaluating the expected long-term field performance of an HPAB. To the best of our knowledge, this is the first study to propose such an application, which could represent a novel, sustainable, and potentially cost-effective strategy for mitigating chlorinated vapour contamination in the subsurface at contaminated sites.

2. Materials and methods

2.1. Materials

Six different carbonaceous materials, comprising three biochar and three coal ashes, were evaluated for the adsorption of TCE in the vapour phase. Feedstocks and production conditions for the available samples, which can influence the materials characteristics (Li et al., 2023; Masud et al., 2023; Yuan et al., 2019; Zhao et al., 2022), were fixed from the producers. The biochar (BC) samples, named MSP550, SWP550 and WSP550, were sourced from the UK Biochar Research Center (UKBRC) and produced from pyrolysis at 550 °C using different biomass feedstocks including miscanthus straw pellets (MSP550), soft wood pellets (SWP550) and wheat straw pellets (WSP550) (Mašek et al., 2018). The coal ash samples, including cyclone coal ash (CA), catchpot coal ash (CP) and thermal activated form of catchpot coal ash (ACP), were obtained from the Institute for Energy and Resource Technology laboratory at Cranfield university. Particularly, the ashes samples were collected from the cyclone or filter units after performing wood pellets gasification at different temperature (700–850 °C). Further information on the production characteristics of all carbonaceous materials is provided in Section S1 of the Supporting Information (Tables S1–S2). TCE (purity ≥99 %, Honeywell, Raunheim, Germany) was used for the adsorption experiments.

2.2. Analytical methods

The elemental composition and the total organic carbon (TOC) of the carbonaceous materials were determined using a CHN-TOC Elementar Analyzer (vario EL CUBE, Elementar). At the end of the analyses, the oxygen content in the samples was calculated by difference (Chen et al., 2021). The CHN-TOC measures were conducted in duplicate using approximately 30 mg of sample. The pH was measured using a pH-meter (JENWAY 4330) by equilibrating 1 g of sample in 20 mL of deionized water for 1.5 h (Xiang et al., 2020).

The morphology of the samples, including particle and pore dimensions, elemental composition and distribution, was analysed by Scanning Electron Microscopy (SEM) (Vega 4, Tescan) equipped with Energy Dispersive X-ray Spectroscopy (EDS) (Aztec INCAx-act, Oxford Instruments).

The surface functional groups were identified through Fourier Transform Infrared Spectroscopy (FTIR) (Alpha II ATR-FTIR spectrometer, Bruker). The analyses were conducted in triplicate, recording the spectra in the range of 4000-400 cm^{-1} with a scan interval of 50–100 scans and a resolution of 4 cm^{-1} (Nair et al., 2022).

Thermogravimetric analysis (TGA) (TGA/DSC 1 STARe System, METTLER TOLEDO) was used to determine moisture content, volatile matter (VM), ash content and fixed carbon (FC). Approximately 45 mg of each sample was used to conduct the analyses. The samples were first heated at 105 °C under N_2 for 10 min to determine the moisture content. Then, the temperature was increased at 10 °C/min to 950 °C and maintained for 10 min under N_2, to determine the VM content. The system was then cooled to 250 °C at the same rate, after which air was introduced and the temperature was again raised to 950 °C at 10 °C/min, maintained for an additional 10 min to quantify the ash content. FC was calculated by difference subtracting the moisture, VM, and ash contents from the initial sample weight and expressing the results as a percentage (Crombie et al., 2013).

TCE concentration in the vapour phase was determined using gas chromatography with a flame ionization detector (GC-FID), specifically a Shimazdu GC_QP2010SE equipped with a Zebron ZB-5 column (30 m × 0.25 mm ID × 0.25 mm film thickness). Helium was used as carrier gas at a flow rate of 0.9 mL min^{-1}, and the oven temperature was programmed to increase from 30 °C to 150 °C at a rate of 8 °C/min (Settimi et al., 2023; Zingaretti et al., 2019). The limit of quantification of TCE using the mentioned method was 0.02 ± 0.001 g m^{-3}. The calibration procedure of the instrument is provided in Section S3.6 of the Supporting Information.

2.3. Experimental setup and procedure for TCE vapour adsorption tests

2.3.1. Batch tests

Batch adsorption tests for TCE vapours were conducted using procedures similar to those adopted in previous studies (Settimi et al., 2023; Zingaretti et al., 2019). The experimental setup is depicted in Fig. S5 of the Supporting Information. The experiments were performed in transparent glass vials, where the carbonaceous material and TCE in vapour phase were introduced. Specifically, a known mass of sorbent was placed at the bottom of each vial, along with a glass tube in which pure TCE was injected. After the injection, the vials were immediately sealed with PTFE/silicone septum caps using a vial crimper, allowing TCE to volatilise in the vial and interact with the sorbent over the test duration. To

account for potential TCE vapour losses unrelated to adsorption, control batch tests (i.e., without carbonaceous material) were conducted in parallel. The average TCE losses observed in the control tests were used to correct the initial TCE vapour concentration in the adsorption capacity calculations.

Several sets of batch experiments were conducted. Initially, equilibrium conditions were assessed by varying both the sorbent mass and exposure time. These preliminary tests, detailed in Section S3.2 of the Supporting Information, led to the selection of 0.01 g of material and a 24-h equilibration time for subsequent experiments.

In the next set of batch tests, comparative adsorption tests were performed on all carbonaceous materials at a fixed TCE vapour concentration of 340 g m^{-3}. These tests were conducted at 20 °C, with temperature control maintained using a thermostatic bath (Buchi B-491 Heating Bath).

Subsequently, adsorption isotherms were determined under varying temperature conditions (5, 20 and 35 °C) and water contents (10 % and 50 % of the saturated water content). Temperature control was achieved using a thermostatic bath for 20 °C and 35 °C, and a laboratory refrigerator for the 5 °C tests, with continuous temperature monitoring via a probe (Hanna Instruments, HI 83141). The tests involving different water contents were carried out at 20 °C.

All the operative conditions used to perform the tests are listed in Table S4, with additional details available in Section S3.1 of the Supporting Information.

At the end of each test, the residual TCE concentration in the vapour phase was measured in the vial headspace using GC-FID (see Section 2.2).

The adsorption capacity of TCE in the vapour phase, denoted as q (g_{TCE} g_{CM}^{-1}) (where CM in the unit refers to the carbonaceous material) was calculated at equilibrium for each sample using Eq. (1) (Pochampally et al., 2023):

$$q = \frac{(C_{ctr} - C_e)\cdot V_v}{m_{CM}} \quad \text{Eq. 1}$$

where C_{ctr} (g m^{-3}) is the theoretical initial TCE vapour concentration, corrected for average losses from control tests, C_e (g m^{-3}) is the residual TCE vapour concentration at equilibrium, V_v (m^3) is the volume of the vial and m_{CM} (g) is the mass of the carbonaceous material used in the test.

2.3.2. Column tests

Column adsorption tests of TCE vapours were performed to evaluate the performances of a sorbent layer over time under dynamic conditions, thus simulating a scenario more representative of HPAB in field applications. The column was filled with a sorbent layer of the biochar named SWP550 that exhibited the highest TCE vapour adsorption capacity among the tested materials (see Fig. 4). SWP550 was used in pellet form, which demonstrated comparable adsorption behaviour to its powdered form (see Section S3.4 of the Supporting Information). The column tests were carried out under diffusive flow conditions, since diffusion is considered the dominant vapour transport mechanism in the unsaturated zone (Verginelli and Yao, 2021; Yao et al., 2013). The experimental set-up, illustrated in Fig. 1, included a glass column equipped with soil gas sampling ports (P0-P5), following the design described by Settimi et al. (2025). From bottom to top, the column was packed as follows: a 10 cm layer of glass beads saturated with pure TCE (serving as the source), a 5 cm layer of clean sand, a 10 cm dry sorbent layer, and a final 11 cm layer of glass beads. The use of pure TCE ensured saturated vapour conditions during the test, with inlet concentrations entering the barrier in the range of approximately 400 g m^{-3} (Cotel et al., 2011). Further details on the column test layout are reported in Section S3.5 of the Supporting Information. The column tests were carried out in duplicate and maintained for 25 days, until sorbent layer saturation was reached. Vapour samples were periodically collected from the sampling

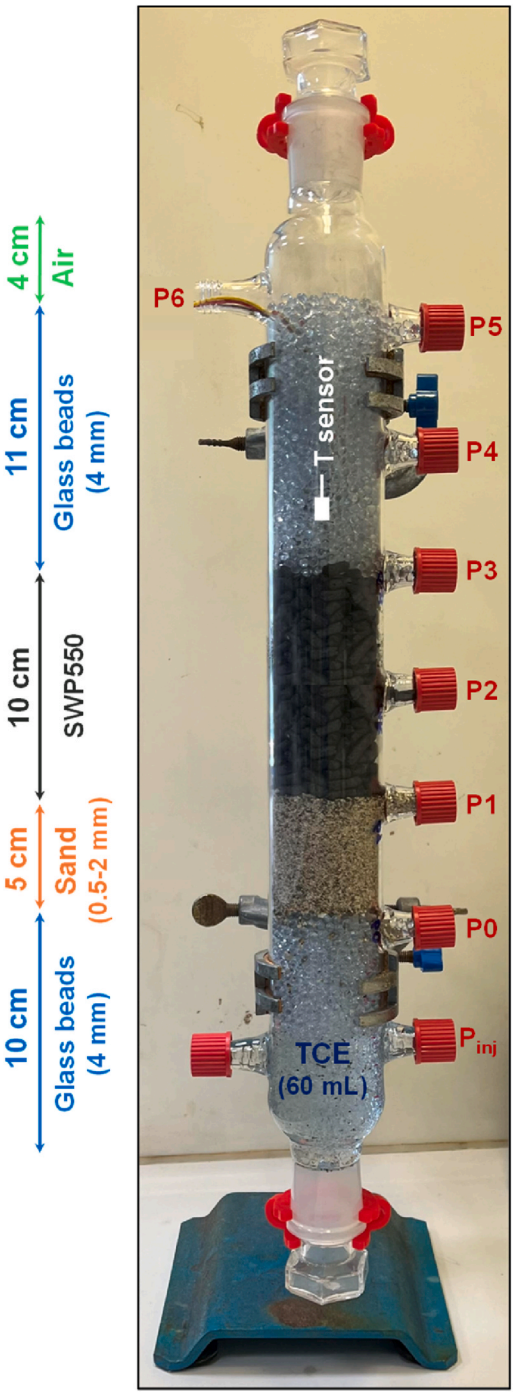

Fig. 1. Layout adopted for column adsorption tests of TCE vapours using biochar SWP550.

ports and analysed using GC-FID, following the analytical procedure described in Section 2.2.

2.4. Adsorption isotherms modelling

Linear and non-linear (i.e., Langmuir and Freundlich) adsorption isotherm models were used to interpret the equilibrium adsorption data obtained from the batch tests. By modelling the experimental data, it was possible to identify the adsorption isotherm model that best described the TCE adsorption in the gas phase for the biochar and the coal ash samples tested.

The linear adsorption model, also known as Henry's model, is

described by the following relationship (Eq. (2)):

$$q = K_{sa} \cdot C_e \quad \text{Eq. 2}$$

where q ($g_{TCE}\ g_{CM}^{-1}$) is the adsorption capacity at equilibrium, C_e is the equilibrium concentration of TCE in the vapour phase (g m^{-3}) and K_{sa} ($m^3\ g^{-1}$) is the linear adsorption constant, which reflects the affinity of the adsorbent material for the adsorbate vapour.

The Langmuir isotherm assumes monolayer adsorption on a surface with a finite number of identical sites, each with the same adsorption energy. This model is represented by Eq. (3):

$$q = \frac{q_m K_L C_e}{1 + K_L C_e} \quad \text{Eq. 3}$$

where q_m ($g_{TCE}\ g_{CM}^{-1}$) is the maximum adsorption capacity and K_L is the Langmuir constant related to the adsorption affinity ($m^3\ g^{-1}$) and C_e (g m^{-3}) is the equilibrium concentration of TCE in the vapour phase (Sadasivam and Reddy, 2015a). The Freundlich adsorption isotherm, on the other hand, is an empirical model that describes adsorption on heterogeneous surfaces with varying adsorption energies, expressed as Eq. (4):

$$q = K_F (C_e)^{\frac{1}{n}} \quad \text{Eq. 4}$$

where K_F ($(g_{TCE}\ g_{CM}^{-1})(m^3\ g_{TCE}^{-1})^{1/n}$) and n (−) are the Freundlich constants related to the capacity and the intensity of adsorption, respectively (Kaikiti et al., 2021).

2.5. HPAB modelling

2.5.1. Analytical modelling

In Fig. 2, the conceptualisation scheme for modelling a HPAB constituted by carbonaceous material is reported. Specifically, the HPAB is placed in the unsaturated zone between the source of contamination and the receptors, such as buildings, to intercept and mitigate the plume of chlorinated vapours. The transport of vapours (1-D, along z direction) in the HPAB is assumed to be governed by diffusion, which is recognised as the dominant transport mechanism of vapours in the unsaturated zone (Yao et al., 2013; Verginelli and Yao, 2021), and is expressed as Eq. (5) (Crank, 1975; Sadasivam and Reddy, 2015a, 2015b):

$$\frac{\partial C}{\partial t} = D_{HPAB} \frac{\partial^2 C}{\partial z^2} - \frac{\partial C_s}{\partial t} \quad \text{Eq. 5}$$

where t (s) is the time, z (m) is the distance, C (g m^{-3}) is the contaminant concentration in the vapour phase and C_s (g m^{-3}) is the equilibrium concentration in the vapour phase after partitioning with the solid phase constituting the barrier, and D_{HPAB} ($m^2\ s^{-1}$) represents the TCE diffusion coefficient in the filling porous media (Millington and Quirk, 1961).

As shown in Section S5 of the Supporting Information, assuming linear adsorption of the vapour phase onto the solid one, Eq. (5) can be written as:

$$R \frac{\partial C}{\partial t} = D_{HPAB} \frac{\partial^2 C}{\partial z^2} \quad \text{Eq. 6}$$

Where R (-) is the retardation factor, which is defined as (Sadasivam and Reddy, 2015a, 2015b):

$$R = 1 + \frac{\rho_{HPAB}}{\theta_{e.HPAB}} K_{sa} \quad \text{Eq. 7}$$

where ρ_{HPAB} (g m^{-3}) is the material bulk density, $\theta_{e.HPAB}$ (−) is the effective porosity of the HPAB and K_{sa} ($m^3\ g^{-1}$) is the linear adsorption constant between the solid adsorbent and the adsorbate in vapour phase. To obtain the analytical solution of Eq. (6), the following boundary conditions were considered (Crank, 1975; Van Genuchten, 1981):

$$\begin{cases} C(z,0) = 0 \\ C(0,t) = C_{in} \\ \dfrac{\partial C(\infty,t)}{\partial z} = 0 \end{cases} \quad \text{Eq. 8}$$

where C_{in} (g m^{-3}) is the TCE concentration in the vapours entering the HPAB. Therefore, the analytical solution of Eq. (6) can be expressed as Eq. (9) (Van Genuchten, 1981):

$$C(z,t) = C_{in}\ erfc\left(\frac{z}{2\sqrt{\frac{D_{HPAB}}{R} \cdot t}}\right) \quad \text{Eq. 9}$$

Therefore, the reported analytical solution assumes that equilibrium is established between the vapour phase and the adsorbed

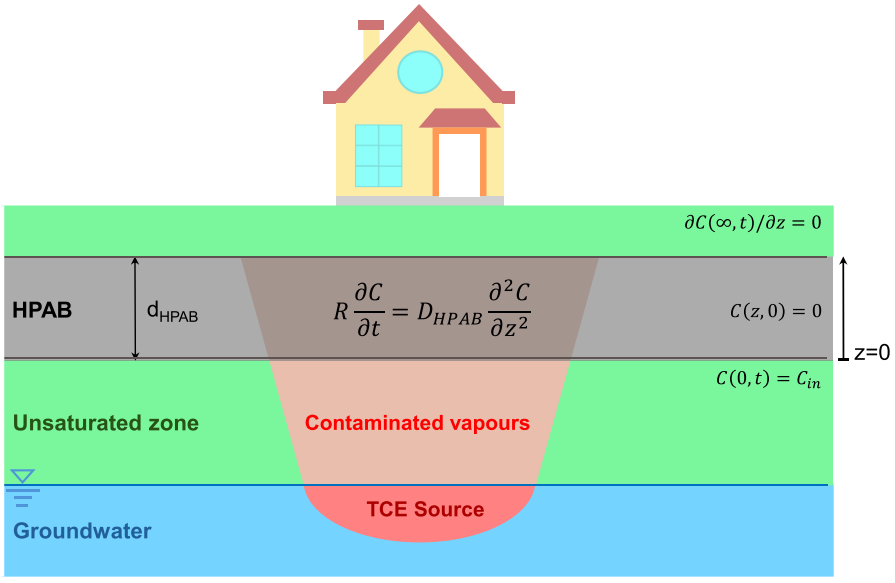

Fig. 2. Conceptualisation of the HPAB model (The z axis is positioned at the top of the HPAB with positive direction towards the surface. The figure also illustrates the boundary conditions used to derive the analytical solution of the vapour transport within the HPAB).

concentration, with a linear adsorption relationship. Further details on the analytical model development (e.g., vapours transport equation derivation, diffusion coefficient estimation) are reported in Section S5 of the Supporting Information.

Using Eq. (9), the normalised concentration of the vapour exiting the HPAB over time can be determined, assuming a constant thickness of the HPAB equal to d_{HPAB} (m):

$$\frac{C(d_{HPAB},t)}{C_{in}} = erfc\left(\frac{d_{HPAB}}{2\sqrt{\frac{D_{HPAB}}{R}.t}}\right) \quad \text{Eq. 10}$$

To provide a preliminary estimate of the barrier's thickness and expected operational lifetime, the time at which the material's adsorption performance declines by a certain percentage (i) was calculated using the following relationship, derived from Eq. (10):

$$t_i = \frac{d_{HPAB}^2}{\frac{4D_{HPAB}}{R}.\left[erf^{-1}\left(1-\frac{C_i}{C_{in}}\right)\right]^2} \quad \text{Eq. 11}$$

Using Eq. (11), the times corresponding to 25 % (t_{25}), 50 % (t_{50}) and 90 % (t_{90}) loss in the material adsorption performance was calculated by assuming the ratio between the concentration exiting and entering the barrier ($\frac{C_i}{C_{in}}$) equal to 0.25, 0.5 and 0.9 respectively:

$$\begin{cases} t_{25} = \dfrac{d_{HPAB}^2}{2.6\dfrac{D_{HPAB}}{R}} \\ t_{50} = \dfrac{d_{HPAB}^2}{0.9\dfrac{D_{HPAB}}{R}} \\ t_{90} = \dfrac{d_{HPAB}^2}{0.03\dfrac{D_{HPAB}}{R}} \end{cases} \quad \text{Eq. 12}$$

2.5.2. Numerical modelling

To simulate the behaviour of an HPAB assuming non-linear adsorption, the vapours transport equation (Eq. (5)) was solved numerically adopting the Langmuir model (Eq. (3)) to describe the adsorption process. Specifically, numerical modelling was used to either derive the adsorption parameters under dynamic conditions from column tests using biochar (see Section 3.5) and estimating the possible HPAB duration as a function of the concentration entering the barrier (see Section 3.6).

The numerical model was implemented using the software COMSOL Multiphysics (COMSOL Inc., Burlington, MA, Version 6.0). Specifically,

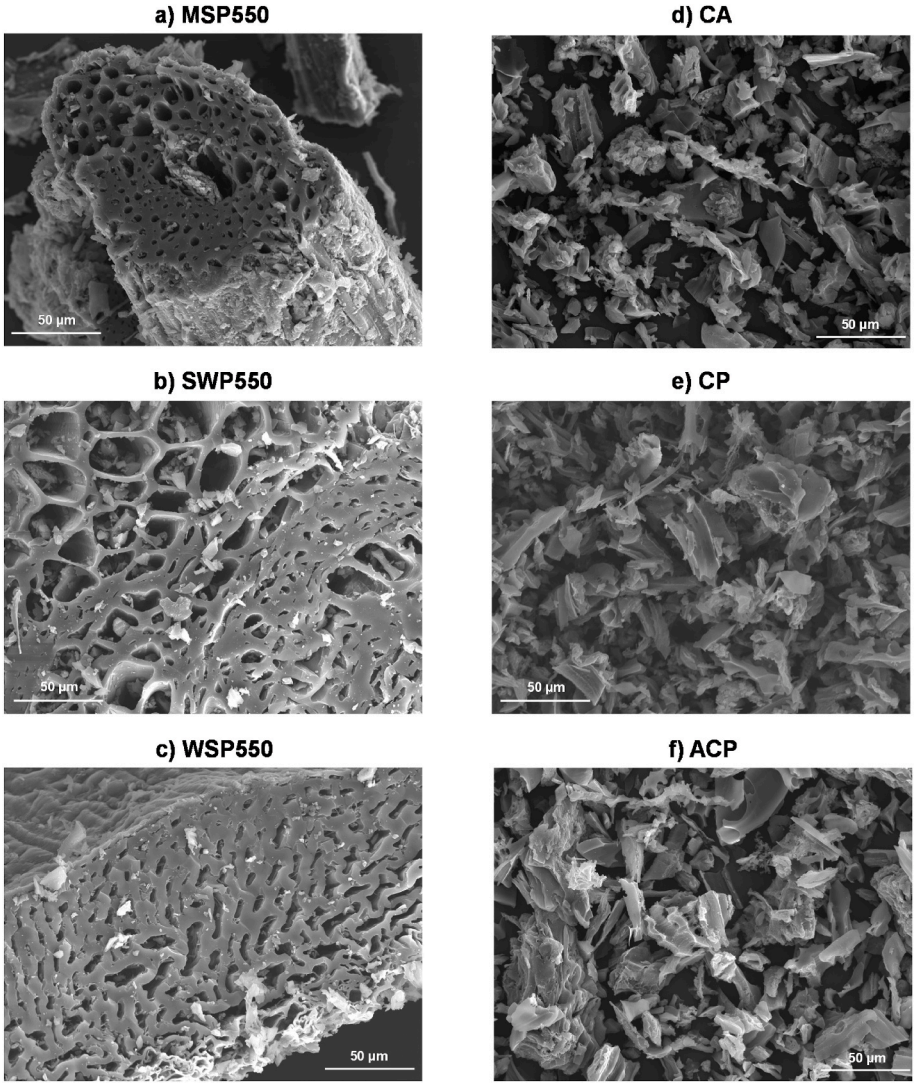

Fig. 3. SEM images of the biochar MSP550 (a), SWP550 (b), WSP550 (c) and of the coal ashes CA (d), CP (e), ACP (f) (1500x magnitude).

a time-dependent study was selected in the software model builder, using the transport of diluted species (tds) module to simulate the vapours transport considering diffusion-dominated transport (Eq. (5)) in porous media. Then, a 1-D geometry was built and boundary conditions were imposed according to different scenarios, such as the column test simulation or the HPAB duration one. Details on the chosen boundary conditions, built geometries, mesh dividing the domain and parameters for modelling the column tests and the HPAB are listed in Table S6 and Table S7 of the Supporting Information, respectively.

3. Results and discussion

3.1. Characterisation of the carbonaceous materials

High magnification SEM images (1500x) of the tested carbonaceous materials (CMs) are shown in Fig. 3, providing a detailed overview of the particles surface. Lower magnification images (150x), offering a broader view of particles morphology and size distribution, are instead provided in Fig. S1 of the Supporting Information. The biochar samples MSP550 (Fig. 3a, Fig. S1a), SWP550 (Fig. 3b, Fig. S1b) and WSP550 (Fig. 3c, Fig. S1c) showed heterogeneous particles in dimension and size (maximum 500 μm), characterised by a porous structure with tubular pores of 4–30 μm diameter. In contrast, the coal ashes samples CA (Fig. 3d, Fig. S1d), CP (Fig. 3e, Fig. S1e) and ACP (Fig. 3f, Fig. S1f) had smoother and rougher particles with smaller dimensions, ranging from 5 to 50 μm, and no visible porosity under SEM analysis.

The main characteristics of the CMs are summarised in Table 1. The elemental analysis showed that the carbon content of the materials ranged from 70 % to 85 %, with SWP550 showing the highest value (86 %). The TOC analysis showed that the carbon contained in all materials is primarily organic. The oxygen content (O) in the samples ranged between 7 and 11 %. The H:C_{org} ratio for all biochar samples ranged between 0.35 and 0.39, while the O:C ratio was below 0.2 for all the materials, indicating a relatively high carbon half-life (Adhikari et al., 2024). These findings are consistent with previous studies on biochar (Adhikari et al., 2024; Rajabi et al., 2021; Vikrant et al., 2020; Trigo et al., 2016) and coal ash characterisation (Benedetti et al., 2018; Galhetas et al., 2014).

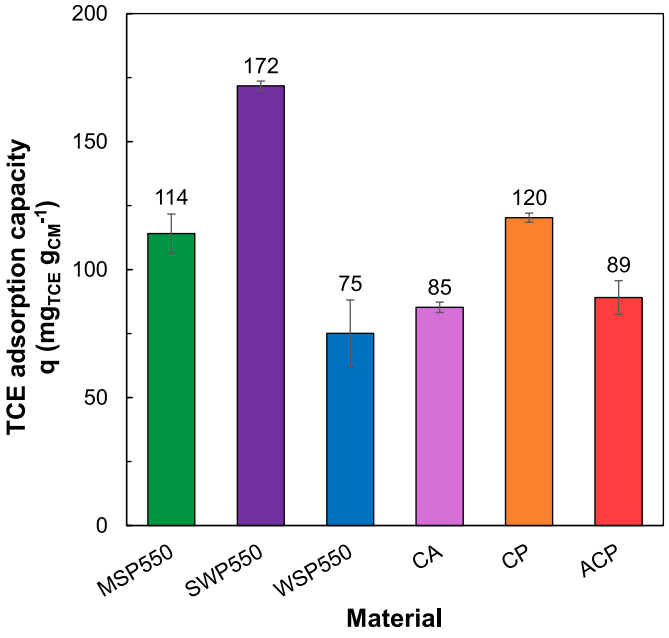

Fig. 4. Adsorption capacity of TCE in the vapour phase using CMs at equilibrium conditions. The error bars represent the standard deviation of the triplicates.

Table 1
Overview of the properties of the carbonaceous materials.

Properties	Carbonaceous Materials (CMs)					
	MSP550	SWP550	WSP550	CA	CP	ACP
C (%wt)	75.4	85.5	68.3	69.5	75.5	77.4
H (%wt)	2.4	2.8	2.1	2.15	2.13	2.3
N (%wt)	0.8	0.1	1.4	0.5	0.6	0.5
O (%wt)	9.2	10.3	6.9	10.9	8.5	9.8
H:C molar ratio (–)	0.4	0.4	0.4	0.37	0.34	0.35
O:C molar ratio (–)	0.09	0.09	0.08	0.12	0.08	0.10
Corg (%wt)	77.7	86.1	68.9	71.4	77.4	79.8
H:C_{org} molar ratio (–)	0.37	0.39	0.37	0.36	0.33	0.34
pH (–)	9.8	7.9	9.9	9.9	9.9	9.7
Moisture (%wt)	4.7	5.1	4.7	4.6	4.8	5.7
VM (%wt)	16.8	16.6	16.5	15.5	17.1	11.7
Ash (%wt)	11.3	2.6	19.6	14.1	11.2	7.8
FC (%wt)	67.1	75.7	59.2	65.8	66.2	74.8
SSA (m^2 g^{-1})	33.6	26.4	26.4	–	–	–

The pH of the CMs was between 9 and 10 which is in agreement with other studies reporting biochar samples characterised by alkaline pH (Yuan et al., 2019; Kaikiti et al., 2021; Xiang et al., 2020; Shen et al., 2018). TGA revealed that all CMs had low moisture levels (≤5 %). The VM content was around 16 % for the biochars and 12–17 % for the coal ashes, reflecting a decrease in VM with increasing production temperature (Zhang et al., 2017b). Fixed carbon (FC) content was high across all materials, ranging from 60 % to 75 %. These results are in line with previous literature on CMs produced under similar conditions (Shen et al., 2018; Vikrant et al., 2020). The values of the specific surface area (SSA) of the biochar samples reported in in Table 1 were provided by UKBRC (Mašek et al., 2018).

Observing FTIR spectra (Fig. S4 of the Supporting Information), biochar samples exhibited different functional groups, generally aliphatic and aromatic C-H, C-C, C=O, and C-O-C groups (Adhikari et al., 2024; Pochampally et al., 2023; Song et al., 2024). In contrast, the coal ash samples exhibited a lower abundance of functional groups, with only low-intensity peaks of aromatic C-C, C-O-C stretching and aromatic C-H.

3.2. Adsorption capacity of the biochar and coal ashes for TCE vapours

Fig. 4 shows the adsorption capacity for TCE vapours obtained in the screening batch tests carried out on the different biochar and coal ash samples. The results indicate that, among the tested materials, SWP550 (biochar) and CP (coal ash) exhibited the highest TCE adsorption capacities. Specifically, among biochar samples, SWP550 achieved a maximum TCE adsorption capacity of 170 mg g^{-1}, while MSP550 and WSP550 showed adsorption capacities of 114 and 90 mg g^{-1}, respectively. Among the coal ash samples, CP showed the highest adsorption capacity of 120 mg g^{-1}, while CA and ACP exhibited similar capacities of approximately 85 and 87 mg g^{-1}, respectively. Taking into account the standard deviations from the adsorption test replicates (represented as error bars in Fig. 4), SWP550 exhibited a significantly higher adsorption capacity compared to the other materials. MSP550 and CP showed comparable performance, whereas WSP550, ACP and CA demonstrated similarly lower adsorption capacities.

The performance of SWP550 aligns with values reported in previous studies on TCE adsorption by carbonaceous materials in both aqueous and vapour phases at room temperature. For instance, Hsu et al. (2014) reported a maximum TCE vapour adsorption capacity of approximately 180 mg g^{-1} using activated carbon derived from seeds, and Erto et al. (2010) observed a TCE adsorption capacity of 160 mg g^{-1} in water by activated carbon.

TCE adsorption is primarily influenced by the polarity of the

compound (Chintawar and Greene, 1997), and several mechanisms may enhance the adsorption process. These include the presence of oxygen functional groups on the surface of the CMs, the electrostatic forces in the active sites and the partitioning mechanism (Zhao et al., 2022; Zhu et al., 2020). Typically, the adsorption of VOCs on biochar is a physical process driven by both surface adsorption onto the carbon fraction and partitioning within the non-volatile organic matter (NOM) (Kaikiti et al., 2021; Zhang et al., 2017b). The NOM content is often associated with the volatile matter (VM) content of the material (Li et al., 2020; Zhang et al., 2017b). Thus, the observed differences in adsorption capacity are attributable to the physicochemical properties of the materials. SWP550, which showed the highest capacity, was rich in organic and fixed carbon, both of which are known to enhance TCE adsorption (Pochampally et al., 2023; Wei and Seo, 2010). Among the coal ashes, CP outperformed the others, likely due to its elevated carbon and VM contents, consistent with previous research indicating that TCE adsorption is enhanced by these factors (Erto et al., 2010; Pochampally et al., 2023; Song et al., 2024).

In general, biochar samples exhibited higher adsorption capacities than coal ashes, which may be attributed to the greater abundance in functional groups (Masud et al., 2023; Song et al., 2024), particularly oxygen functional groups such as C-O-C and C=O, which are known to promote TCE adsorption (Ahmad et al., 2012; Erto et al., 2010; Yang et al., 2019). Such groups can in fact increase the surface polarity of biochar, thus enhancing adsorption of polar molecules, like TCE (Almazán-Almazán et al., 2007; Sadegh et al., 2024). Based on the results of these preliminary tests, SWP550 and CP were identified as the most effective materials for TCE adsorption and were selected for further investigation.

3.3. TCE vapour adsorption isotherms at varied temperatures

The TCE vapours adsorption isotherms obtained for SWP550 and CP at the temperature of 5 °C, 20 °C and 35 °C are shown in Fig. 5. Across the tested temperatures, the TCE vapour adsorption capacity of SWP550 (Fig. 5a–c) was consistently higher than that of CP (Fig. 5d–f). Both materials showed a decrease in adsorption capacity with increasing temperature (Fig. 5). Specifically, the adsorption capacity remained relatively stable between 5 °C and 20 °C, with a more noticeable decrease occurring between 20 °C and 35 °C. In particular, the maximum values of TCE vapour adsorption capacity for the biochar SWP550 resulted around 180 mg g^{-1}, 170 mg g^{-1} and 150 mg g^{-1} with increasing temperature from 5 °C to 20 °C and 35 °C respectively (Fig. 5a–c), thus resulting in a loss of the adsorption capacity of 5 % among 5 °C and 20 °C and 13 % among 20 °C and 35 °C. Furthermore, for the coal ash CP the maximum values of TCE vapour adsorption capacity resulted around 110 mg g^{-1} for 5 °C and 20 °C and decreased to 90 mg g^{-1} increasing temperature to 35 °C (Fig. 5d–f), thus resulting in a loss of the adsorption capacity of around 18 % from 5 °C to 35 °C.

This temperature-dependent decrease is likely due to the exothermic nature of adsorption, where the increased molecular energy at higher temperatures diminishes the efficiency of the physical adsorption forces involved (Erto et al., 2010; Nikam and Mandal, 2020). These observations are in agreement with other studies on TCE adsorption. For example, Erto et al. (2010) reported a decrease in TCE adsorption capacity on activated carbon when the temperature was increased from 10 °C to 50 °C, while Nikam and Mandal (2020) observed minimal changes in adsorption between 30 °C and 50 °C.

Both SWP550 and CP samples showed a non-linear adsorption trend, which is consistent with previous studies on chlorinated solvents adsorption on activated carbon particles in both the gas phase (Hsu et al., 2014; Nikam and Mandal, 2020) and water phase (Ahmad et al., 2012). To interpret the adsorption data, Langmuir (Eq. (3)) and Freundlich (Eq. (4)) non-linear models were applied. The fitted trends, along with the experimental data, are presented in Fig. 5. To improve the quality of the fitting and better represent the overall adsorption behaviour also at higher concentrations, data corresponding to TCE vapour equilibrium concentrations below 10 g m^{-3} were excluded from

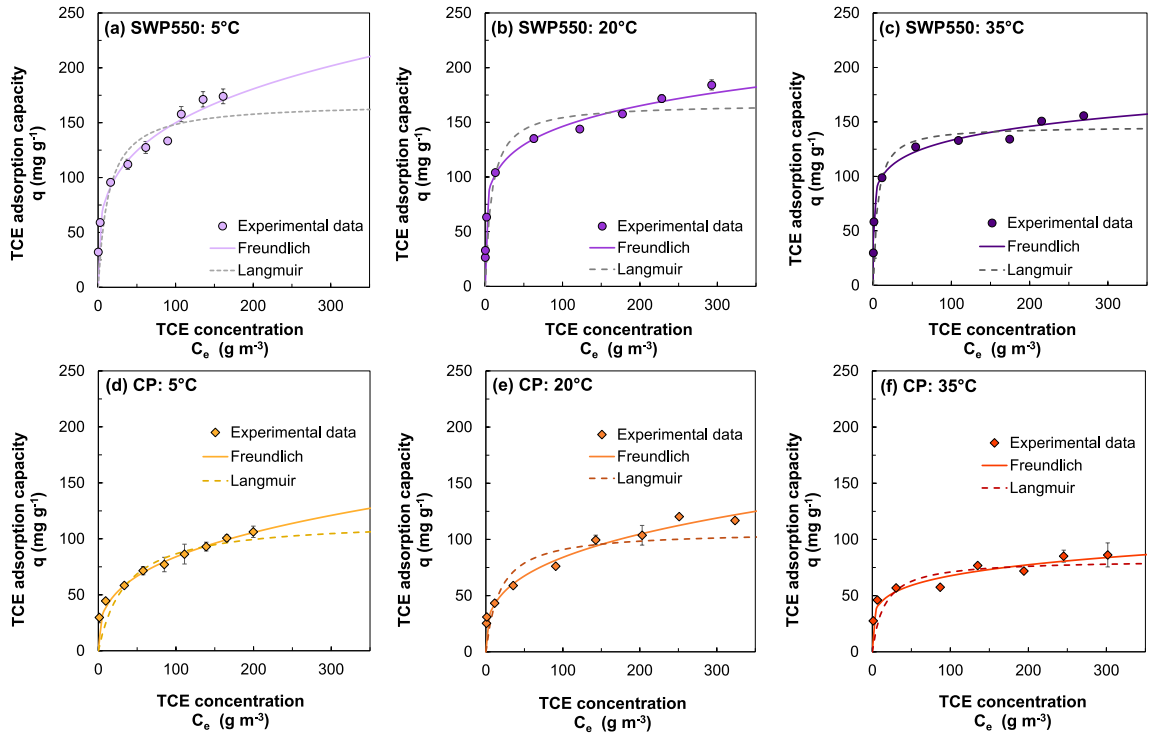

Fig. 5. TCE vapour adsorption capacity as a function of TCE equilibrium concentration in the vapour phase at different temperatures for biochar SWP550 for (a) 5 °C, (b) 20 °C, (c) 35 °C and the coal ash CP for (d) 5 °C, (e) 20 °C and (f) 35 °C. The error bars represent the standard deviation of duplicate measurements. The Freundlich and Langmuir adsorption isotherm models (solid and dotted lines, respectively) are also included.

the analysis.

Overall, both Langmuir and Freundlich models exhibit a good fit with the experimental data (see the statistical indexes values in Table 2), with the Freundlich model showing slightly better correlation. As shown in Table 2, the Freundlich constant (K_F) values increased across different temperatures, ranging from 43 to 72 (mg g^{-1})(m^3 mg^{-1})$^{1/n}$ for SWP550 and from 18 to 27 (mg g^{-1})(m^3 mg^{-1})$^{1/n}$ for CP, indicating a change in the adsorption performances. The values of the Freundlich exponent n ranged from 3 to 8 for all materials, suggesting non-linear adsorption behaviour. These results indicate that the adsorption of TCE in the gas phase onto the tested carbonaceous materials is a physical and reversible process, leading to the formation of a molecular multilayer on the surface of both biochar and coal ash (Erto et al., 2010; Manap et al., 2018; Nikam and Mandal, 2020; Tan et al., 2024).

3.4. TCE vapour adsorption isotherms at varied water content

The effect of water content on the adsorption of TCE vapours using SWP550 and CP was studied by adding different quantities of water into the materials used in the tests. In particular, tests were performed with 10 % and 50 % of the saturated water content of the samples evaluated as described in Section S3.3 of the Supporting Information. The adsorption tests were performed at ambient temperature (20 °C) following the layout depicted in Fig. S5 and described in Section 2.3.1.

The TCE vapours adsorption isotherms obtained at the different water contents are shown in Fig. 6. The results obtained at 20 °C without adding water in the vials are also shown as reference. It can be noticed that the addition of water reduced the TCE adsorption capacity in both materials. In particular, the maximum values of TCE vapour adsorption capacity for the biochar SWP550 resulted around 130 mg g^{-1} and 115 mg g^{-1} with 10 % and 50 % of saturated water content of the material, respectively (Fig. 6b and c). Conversely, without any addition of water, SWP550 registered a TCE vapour adsorption capacity of around 180 mg g^{-1} (Fig. 6a). For the coal ash CP, the TCE vapour adsorption capacity resulted around 86 mg g^{-1} and 82 mg g^{-1} with water at 10 % and 50 % of the saturated water content on the material, respectively (Fig. 6e and f) while without any addition of water, the maximum adsorption capacity of TCE in gas phase on CP resulted 120 mg g^{-1} (Fig. 6d). Therefore, a loss in adsorption performances of around 30 % was observed by increasing the water content on both the tested materials. These results are in agreement with the findings of Jia et al. (2020) for the adsorption of TCE vapours onto activated carbons, or with the ones of Sadasivam and Reddy (2015a) for the adsorption of methane on biochar and activated carbon.

Non-linear behaviour was observed in the adsorption trends, even in the presence of water. Consequently, the Langmuir and Freundlich models were applied to the experimental data, resulting in the parameters reported in Table 2 and in Fig. 6 in addition to the experimental data obtained from the adsorption tests. Freundlich adsorption isotherm resulted characterised by higher correlation than Langmuir one (see statistical indexes values in Table 2). The biochar SWP550 led to values of the Freundlich constant K_F equal to 62 and 42 (mg g^{-1})(m^3 mg^{-1})$^{1/n}$ for moisture equal to 10 and 50 % of saturated water content, respectively. Instead, the coal ash CP reached values of K_F around 18 (mg g^{-1}) (m^3 mg^{-1})$^{1/n}$ at 10 and 50 % of saturation. These values were slightly lower than the ones obtained by modelling Freundlich isotherms for the experimental data at the same temperature without added water, for which K_F resulted 65 and 19 (mg g^{-1})(m^3 mg^{-1})$^{1/n}$ for the SWP550 and CP, respectively (see Table 2).

Notably, from the experimental results, increasing moisture resulted in a greater decrease in the TCE vapours adsorption capacity compared to increasing temperature. This result agrees with Sadasivam and Reddy (2015a), who observed similar behaviour of methane adsorption capacity on biochar and activated carbon, which decreased as a function of moisture rather than temperature.

Generally, the decrease of the TCE adsorption capacity with increasing moisture may depend on the fact that the water molecules could occupy part of the active sites in the materials, otherwise available for TCE adsorption. Thus, the presence of water could hinder the partition mechanism of TCE on the materials. In fact, if the water content increases, the pore volume will decrease with a consequent decrease in the adsorption capacity (Jia et al., 2020). This could be due to the ability of water to form hydrogen bonds with polar functional groups, resulting in blockage of pore access for TCE (Li et al., 2021a; Yang et al., 2019). Furthermore, the presence of oxygen functional groups, such as C=O and C-O-C, can decrease TCE adsorption in the presence of water (Ahmad et al., 2012; Erto et al., 2010; Yang et al., 2019).

3.5. TCE vapour adsorption in column

Fig. 7 shows the normalised TCE vapour concentration profiles detected in the column tests relative to the inlet (P1, Fig. 7a), the midpoint (P2, Fig. 7b), and the outlet of the sorbent layer (P3, Fig. 7c), plotted as breakthrough curves over time. The concentrations of TCE detected in the different sampling ports (P1-P3) were normalised to the concentration of 400 g m^{-3}, aligned with the average measured concentration at the port P0.

Under the tested conditions, the experimental breakthrough curves reached a plateau at approximately 350 h for vapours detected in the middle of the sorbent layer (Fig. 7b) and at around 400 h for vapours exiting the barrier (Fig. 7c), indicating that HPAB had reached saturation. This behaviour is consistent with a non-linear adsorption process, as previously observed in the batch test results.

To quantify this non-linear adsorption behaviour under dynamic conditions, the experimental data obtained from the column tests were used to calibrate the numerical model developed in COMSOL Multiphysics (see Section 2.5.2). The Langmuir constant (K_L) and maximum adsorption capacity (q_m) served as fitting parameters. The input data used for the model fitting are reported in Section S3.5 of the Supporting Information (Table S6). The modelled breakthrough curves, shown as

Table 2
Langmuir and Freundlich adsorption isotherm parameters and regression coefficient of determination (R^2) for TCE vapour adsorption on biochar SWP550 and coal ash CP at 5, 20 and 35 °C and at 10 %sat and 50 %sat water contents, derived from batch tests.

Material	Temperature	Water content	Langmuir model parameters				Freundlich model parameters			
			q_m (mg g^{-1})	K_L (m^3g^{-1})	R^2	NMRSE	n (−)	K_F ((mg g^{-1})(m^3mg^{-1})$^{1/n}$)	R^2	NMRSE
SWP550	5 °C	–	168.29	0.07	0.84	0.095	3.71	43.31	0.95	0.048
	20 °C	–	167.01	0.12	0.88	0.076	5.70	65.15	0.97	0.030
	35 °C	–	146.04	0.18	0.90	0.053	7.53	72.21	0.95	0.033
	20 °C	10 %sat	115.80	0.21	0.70	0.076	8.61	62.49	0.85	0.049
	20 °C	50 %sat	107.39	0.09	0.77	0.081	5.84	42.20	0.87	0.054
CP	5 °C	–	116.88	0.03	0.96	0.046	3.01	18.15	0.99	0.015
	20 °C	–	107.33	0.06	0.90	0.136	3.16	19.53	0.98	0.053
	35 °C	–	81.94	0.06	0.65	0.092	5.10	27.44	0.80	0.066
	20 °C	10 %sat	70.79	0.08	0.75	0.017	3.82	17.90	0.94	0.074
	20 °C	50 %sat	70.80	0.08	0.74	0.133	4.02	18.92	0.94	0.055

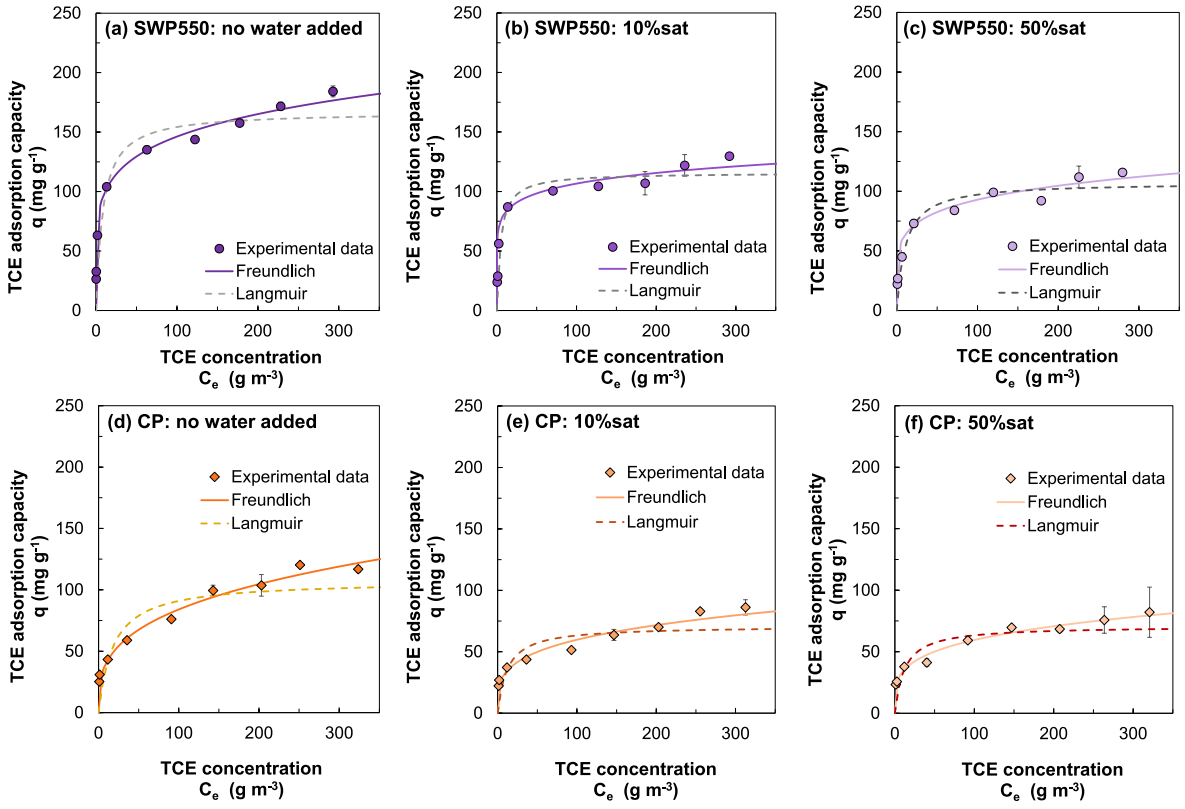

Fig. 6. TCE vapour adsorption capacity at 20 °C as a function of equilibrium concentration of TCE in the gas phase for different water contents using the biochar SWP550 for (a) no addition of water, (b) 10 %sat, (c) 50 %sat and the coal ash CP for (d) no addition of water, (e)10 %sat and (f) 50 %sat. The error bars shown in the figures represent the standard deviation of the different replicates of the tests. Freundlich and Langmuir adsorption isotherm models (solid and dotted lines, respectively) are also included.

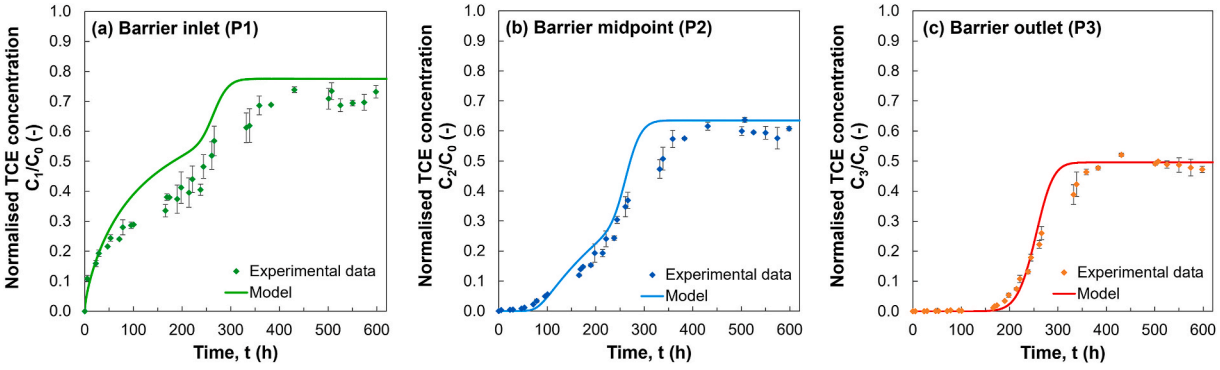

Fig. 7. Normalised TCE concentration profiles in the column for vapours analysed at P1 (a), P2 (b) and P3 (c). Indicators represent experimental data with error bars indicating the standard deviation of the duplicate. Solid lines represent the modelled trend assuming Langmuir adsorption.

solid lines in Fig. 7, demonstrated a good match with the experimental data, with normalised root-mean-square error (NRMSE) of 0.11 (Fig. 7a and b) and 0.15 (Fig. 7c). The values of Langmuir fitting parameters were 0.06 $m^3\ g^{-1}$ for the Langmuir constant (K_L) and 100 mg g^{-1} for the maximum adsorption capacity (q_m). These values are consistent with the results observed using SWP550 in both powder (see Table 2) and pellet form (see Table S5 of the Supporting Information). These findings therefore support the reliability of the batch test methodology and highlight the potential effectiveness of using these adsorbent materials as horizontal permeable adsorptive barriers (HPABs) for mitigating subsurface vapour intrusion. As also highlighted in Section 2.3.2, it should be acknowledged that the performed column adsorption tests present limitations in simulating field-like HPAB environment as they do not account for factors, e.g., biological activity or soil heterogeneity, that could influence the adsorption process.

3.6. Estimation of HPAB duration

The column test results, discussed in the previous section, demonstrated the feasibility of employing the tested adsorbent materials as HPABs for vapour mitigation. In these tests, a pure TCE vapour source was simulated, resulting in barrier lifespans of approximately one month due to the high concentrations used (i.e., saturation conditions). To better resemble typical field conditions, where vapour concentrations are significantly lower than saturation, numerical simulations were conducted to estimate the long-term performance of HPABs. These

simulations used the adsorption parameters derived from column experiments performed with biochar SWP550 and evaluated barrier lifespan under various source concentrations (see Table S7 for modelling parameters) as a function of barrier thickness (d_{HPAB}).

In these simulations a range of TCE vapour concentrations at the source, varying from 1 to 100 g m^{-3}, was considered to reflect typical field scenarios. It is important to note that for concentrations equal to 1 g m^{-3} and a Langmuir constant (K_L) of 0.06 m^3 g^{-1} the denominator in the Langmuir model (Eq. (3)) approaches unity (i.e., $1 + K_L \cdot C_e \approx 1$), thereby reducing the adsorption model to the form of Henry's isotherm (Eq. (2)):

$$q\ (low\ concentrations) = \frac{q_m K_L C_e}{1 + K_L C_e} \approx q_m K_L C_e \approx K_{sa} C_e \qquad \text{Eq. 13}$$

In such case, the linear adsorption constant K_{sa} can be therefore defined as:

$$K_{sa} = K_L \cdot q_m \qquad \text{Eq. 14}$$

In this specific case, assuming a K_L equal to 0.06 m^3 g^{-1} and q_m equal to 100 mg g^{-1}, the resulting linear adsorption constant K_{sa} is equal to 0.006 m^3 g^{-1}, which effectively approximates the adsorption behaviour for concentrations equal to or lower than 1 g m^{-3}. Under these conditions, the barrier lifetime becomes independent of the source concentration, and the analytical model described in Section 2.5.1 can be applied (see Eq. (12)).

The modelling results are presented in Fig. 8, for low and high contamination scenarios. Fig. 8a reports the HPAB lifetime as a function of the barrier thickness for TCE concentrations ≤1 g m^{-3}, indicating the time to reach 25 %, 50 %, and 90 % material saturation. For a barrier thickness of 0.5 m, the estimated half-life (t_{50}) is approximately 15 years, suggesting long-term performance. Such estimated HPAB duration is compatible with the carbon half-life in soil (>1000 years), as indicated by the O:C ratio of the carbonaceous material (Adhikari et al., 2024). The analytical solution, based on the assumption of a linear distribution (see dot markers in Fig. 8), closely approximates the trends predicted by the non-linear numerical model for concentrations lower than 1 g m^{-3}. The slight discrepancies observed between the two approaches can be attributed to the boundary condition imposed in the analytical model, which assumes no flux conditions at $z \rightarrow \infty$. Further comparisons between the analytical and numerical results are provided in Section S6 of the Supporting Information. Fig. 8b reports the expected half-life of the barrier (t_{50}) for concentrations ranging from 1 to 100 g m^{-3}. As expected, due to the non-linear adsorption behaviour described by the Langmuir model, the HPAB lifetime decreases significantly with increasing TCE concentration. Specifically, t_{50} values drop to approximately 10 years at 10 g m^{-3} and to 3 years at 100 g m^{-3}, highlighting the influence of vapour concentrations on barrier longevity.

It is important to note that a vapour concentration in the source equal to or below 1 g m^{-3} is representative of conditions commonly found at many contaminated sites. Notably, this value corresponds to a concentration in the vapour phase 500 times higher than 0.002 g m^{-3} that is the soil vapour concentration achievable considering a TCE concentration in groundwater equal 0.005 mg L^{-1}, i.e., the U.S. EPA Maximum Contaminant Level (MCL) (U.S. EPA, 2007), assuming a dimensionless Henry's law constant of 0.403 (U.S. EPA, 2024). Thus, the use of a simplified analytical model at low concentrations (<1 g m^{-3}) proves to be a valuable tool for rapid and reliable estimation of HPAB performance, showing good agreement with the numerical modelling results.

It should further be noted that the developed models did not fully consider field complexities, such as porous media heterogeneity or variability of environmental conditions, that can occur in HPAB real conditions.

4. Conclusions

This study demonstrates the potential of biochar and coal ashes for the adsorption of TCE vapours. Among the tested materials, the biochar named SWP550 and the coal ash named CP exhibited the highest adsorption capacities, ranging from 75 to 170 mg_{TCE} g_{CM}^{-1}. Namely, SWP550 showed the highest adsorption capacity likely due its higher carbon content. Both SWP550 and CP were evaluated across different temperatures (i.e., 5, 20 and 35 °C) and water contents (10 % and 50 % of the saturated water content). The results showed a decrease in TCE vapour adsorption capacity with increasing temperature and water content, aligning with prior studies on activated carbon-based adsorption on both gas and aqueous phases (Erto et al., 2010; Jia et al., 2020; Manap et al., 2018; Nikam and Mandal, 2020). The adsorption data further revealed a non-linear increase in TCE adsorption with increasing vapour concentration, and the Freundlich isotherm provided the best fit to describe the adsorption process. This supports the conclusion that TCE adsorption on these materials is primarily a physical process.

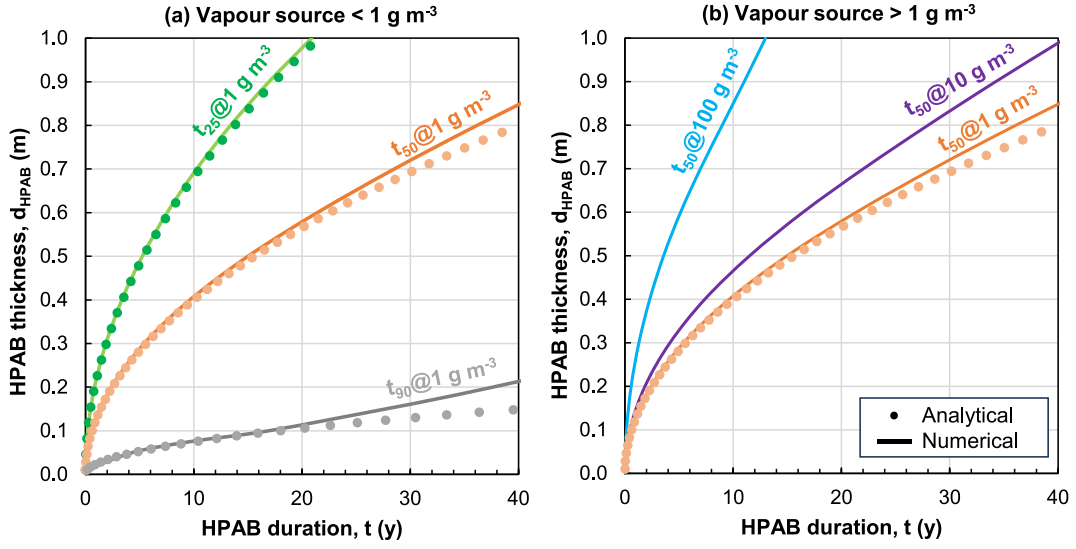

Fig. 8. Estimation of the HPAB duration for biochar SWP550 as a function of its thickness at (a) low and (b) high concentration values. The solid lines represent the data obtained by numerical modelling assuming Langmuir isotherm while the dots represent the duration estimated with the analytical modelling assuming linear adsorption (Eq. (12)).

Non-linear adsorption behaviour was also observed by performing column adsorption tests at dynamic conditions using biochar SWP550, showing to maintain good levels of TCE adsorption capacity. Integrating the experimental data obtained from column tests into a numerical model developed in COMSOL Multiphysics revealed that barriers composed with biochar (SWP550) could achieve a half-life duration of over 15 years with a thickness of 0.5 m, assuming TCE vapour concentrations entering the barrier up to 1 g m^{-3} (i.e., 500 times higher than the MCL). By increasing the concentration of TCE entering the barrier to 10–100 g m^{-3}, the half-life duration of the 0.5 m-thick HPAB decreased to 3–10 years, thus suggesting that an increase in thickness may be needed in case of high levels of contamination. The results indicate the potential of carbonaceous materials as durable passive sorbent solutions for managing TCE vapour emissions in the unsaturated zone. Overall, this study provides a novel contribution to the field of environmental remediation by demonstrating that biochar and coal ash not only serve as effective adsorbents for chlorinated solvent vapours but also as promising candidates for passive remediation strategies for contaminated sites. These findings highlight the significant potential of these low-cost, sustainable materials in advancing risk management and remediation strategies for chlorinated solvent contamination.

Nomenclature

Symbol	Parameter	Unit
AC	Activated carbon	–
ACP	Activated catchpot coal ash from wood pellets gasification	–
BC	Biochar	–
CA	Cyclone coal ash from wood pellets gasification	–
C_{ctr}	Contaminant concentration in the control test	[M/L^3]
C_e	Contaminant concentration in the vapour phase at equilibrium	[M/L^3]
C_{in}	Contaminant initial vapour concentration	[M/L^3]
CMs	Carbonaceous materials	–
CP	Catchpot coal ash from wood pellets gasification	–
C_s	Contaminant concentration in the solid phase	[M/L^3]
CVOCs	Chlorinated Volatile Organic Compounds	–
D_{HPAB}	Effective diffusion coefficient in the HPAB	[L^2/T]
DNAPL	Dense Non-aqueous Phase Liquid	–
D_{TCE}	TCE air diffusion coefficient	[L^2/T]
d_{HPAB}	HPAB thickness	[L]
EDS	Energy Dispersive Spectroscopy	–
FC	Fixed carbon	–
FTIR	Fourier Infrared Spectroscopy	–
GC-FID	Gas chromatography with Flame Ionization Detector	–
HPAB	Horizontal Permeable Adsorbing Barrier	–
HVOCs	Halogenated Volatile Organic Compounds	–
K_F	Freundlich constant	[$(M/M)(L^3/M)^{1/n}$]
K_L	Langmuir constant	[L^3/M]
K_{sa}	Linear adsorption constant	[L^3/M]
MCL	Maximum Contaminant Level	–
m_{CM}	Mass of carbonaceous material	–
MSP550	Biochar from Miscanthus pellets produced at 550 °C pyrolysis	–
n	Freundlich exponent	[-]
NOM	Non-volatile organic matter	–
NRMSE	Normalised root-mean square error	[-]
Q	Adsorption capacity	[M/M]
q_m	Langmuir maximum adsorption capacity	[M/M]
R	Retardation factor	[-]
R^2	Coefficient of determination	[-]
SSA	Surface Specific Area	–
SEM	Scanning Electron Microscopy	–
SWP550	Biochar from Softwood pellets produced at 550 °C pyrolysis	–
TCE	Trichloroethylene	–
TGA	Thermogravimetric Analysis	–
TOC	Total Organic Carbon	[-]
$t_{25,50,90}$	Time for HPAB consumption of 25,50,90 %	[T]
VM	Volatile matter	–
VOCs	Volatile Organic Compounds	–
V_v	Vial volume	[L^3]
WSP550	Biochar from Wheat straw pellets produced at 550 °C pyrolysis	–
ρ_{HPAB}	Bulk density of the material filling the HPAB	[M/L^3]
$\theta_{e.HPAB}$	Effective porosity of HPAB	[-]

(continued on next column)

(continued)

CRediT authorship contribution statement

Clarissa Settimi: Writing – original draft, Methodology, Formal analysis, Data curation, Conceptualization. **Benedetta Conti:** Writing – original draft, Methodology, Investigation, Formal analysis, Data curation. **Iason Verginelli:** Writing – review & editing, Supervision, Resources, Methodology, Conceptualization. **Daniela Zingaretti:** Writing – review & editing, Supervision, Methodology, Conceptualization. **Immacolata Bortone:** Writing – review & editing. **Frederic Coulon:** Writing – review & editing, Supervision, Resources, Funding acquisition, Conceptualization. **Renato Baciocchi:** Writing – review & editing, Supervision, Resources, Project administration, Funding acquisition, Conceptualization.

Declaration of competing interest

The authors declare the following financial interests/personal relationships which may be considered as potential competing interests: Frederic Coulon and Immacolata Bortone reports financial support was provided by Biotechnology and Biological Sciences Research Council (BBSRC) NIBB's Environmental Biotechnology Network.

Acknowledgments

The authors would like to thank Prof. Kumar Patchigolla from the Institute for Energy and Resource Technology of Cranfield University for providing the coal ash samples, Cadia d'Ottavi from the Department of Chemical Science and Technologies of the University of Rome Tor Vergata for the TGA analyses and Nicolò Tonolo from the Department of Civil Engineering and Computer Science Engineering of the University of Rome Tor Vergata for the temperature monitoring with sensors. The authors would like to acknowledge the financial support of the Biotechnology and Biological Sciences Research Council (BBSRC) NIBB's Environmental Biotechnology Network (EBNET, grant reference BB/S009795/1).

Appendix A. Supplementary data

Supplementary data to this article can be found online at https://doi.org/10.1016/j.jenvman.2025.126501.

Data availability

Data will be made available on request.

References

Adhikari, S., Moon, E., Paz-Ferreiro, J., Timms, W., 2024. Comparative analysis of biochar carbon stability methods and implications for carbon credits. Sci. Total Environ. 914, 169607. https://doi.org/10.1016/j.scitotenv.2023.169607.

Ahmad, M., Lee, S.S., Dou, X., Mohan, D., Sung, J.-K., Yang, J.E., Ok, Y.S., 2012. Effects of pyrolysis temperature on soybean stover- and peanut shell-derived biochar properties and TCE adsorption in water. Bioresour. Technol. 118, 536–544. https://doi.org/10.1016/j.biortech.2012.05.042.

Ahmad, M., Rajapaksha, A.U., Lim, J.E., Zhang, M., Bolan, N., Mohan, D., Vithanage, M., Lee, S.S., Ok, Y.S., 2014. Biochar as a sorbent for contaminant management in soil and water: a review. Chemosphere 99, 19–33. https://doi.org/10.1016/j.chemosphere.2013.10.071.

Alhashimi, H.A., Aktas, C.B., 2017. Life cycle environmental and economic performance of biochar compared with activated carbon: a meta-analysis. Resour. Conserv. Recycl. 118, 13–26. https://doi.org/10.1016/j.resconrec.2016.11.016.

Almazán-Almazán, M.C., Pérez-Mendoza, M., Domingo-García, M., Fernández-Morales, I., Del Rey-Bueno, F., García-Rodríguez, A., López-Garzón, F.J., 2007. The role of the porosity and oxygen groups on the adsorption of n-alkanes, benzene, trichloroethylene and 1,2-dichloroethane on active carbons at zero surface coverage. Carbon 45, 1777–1785. https://doi.org/10.1016/j.carbon.2007.05.003.

An, X., Wang, Y., Yu, C., Hu, X., 2024. Biochar-bacteria coupling system enhanced the bioremediation of phenol wastewater-based on life cycle assessment and environmental safety analysis. J. Hazard. Mater. 480, 136414. https://doi.org/10.1016/j.jhazmat.2024.136414.

Balsamo, M., Di Natale, F., Erto, A., Lancia, A., Montagnaro, F., Santoro, L., 2013. Gasification of coal combustion ash for its reuse as adsorbent. Fuel 106, 147–151. https://doi.org/10.1016/j.fuel.2012.11.077.

Benedetti, V., Patuzzi, F., Baratieri, M., 2018. Characterization of char from biomass gasification and its similarities with activated carbon in adsorption applications. Appl. Energy 227, 92–99. https://doi.org/10.1016/j.apenergy.2017.08.076.

Chavan, D., Kumar, S., 2018. Reduction of methane emission from landfill using biocover as a biomitigation system: a review. Indian J. Exp. Biol.

Chen, Jiefeng, Wang, P., Ding, L., Yu, T., Leng, S., Chen, Jie, Fan, L., Li, Jingjing, Wei, L., Li, Jun, Lu, Q., Leng, L., Zhou, W., 2021. The comparison study of multiple biochar stability assessment methods. J. Anal. Appl. Pyrolysis 156, 105070. https://doi.org/10.1016/j.jaap.2021.105070.

Chintawar, P.S., Greene, H.L., 1997. Adsorption and catalytic destruction of trichloroethylene in hydrophobic zeolites. Appl. Catal. B Environ. 14, 37–47. https://doi.org/10.1016/S0926-3373(97)00010-6.

Cotel, S., Schäfer, G., Barthes, V., Baussand, P., 2011. Effect of density-driven advection on trichloroethylene vapor diffusion in a porous medium. Vadose Zone J. 10, 565–581. https://doi.org/10.2136/vzj2010.0032.

Crank, J., 1975. The Mathematics of Diffusion, 2d ed. Clarendon Press, Oxford.

Crombie, K., Mašek, O., Sohi, S.P., Brownsort, P., Cross, A., 2013. The effect of pyrolysis conditions on biochar stability as determined by three methods. GCB Bioenergy 5, 122–131. https://doi.org/10.1111/gcbb.12030.

Da Silva Santos, D.H., Paulino, J.C.P.L., Dos Santos Alves, G.F., De Magalhães Oliveira, L. M.T., De Carvalho Nagliate, P., Da Silva Duarte, J.L., Meili, L., Tonholo, J., Zanta, C. L.D.P.E.S., 2021. Effluent treatment using activated carbon adsorbents: a bibliometric analysis of recent literature. Environ. Sci. Pollut. Res. 28, 32224–32235. https://doi.org/10.1007/s11356-021-14267-w.

Damgaard, I., Bjerg, P.L., Bælum, J., Scheutz, C., Hunkeler, D., Jacobsen, C.S., Tuxen, N., Broholm, M.M., 2013. Identification of chlorinated solvents degradation zones in clay till by high resolution chemical, microbial and compound specific isotope analysis. J. Contam. Hydrol. 146, 37–50. https://doi.org/10.1016/j.jconhyd.2012.11.010.

Erto, A., Andreozzi, R., Di Natale, F., Lancia, A., Musmarra, D., 2010. Experimental and statistical analysis of trichloroethylene adsorption onto activated carbon. Chem. Eng. J. 156, 353–359. https://doi.org/10.1016/j.cej.2009.10.034.

Galhetas, M., Mestre, A.S., Pinto, M.L., Gulyurtlu, I., Lopes, H., Carvalho, A.P., 2014. Carbon-based materials prepared from pine gasification residues for acetaminophen adsorption. Chem. Eng. J. 240, 344–351. https://doi.org/10.1016/j.cej.2013.11.067.

Hsu, S.-H., Huang, C.-S., Chung, T.-W., Gao, S., 2014. Adsorption of chlorinated volatile organic compounds using activated carbon made from Jatropha curcas seeds. J. Taiwan Inst. Chem. Eng. 45, 2526–2530. https://doi.org/10.1016/j.jtice.2014.05.028.

Huang, X., Tang, M., Li, H., Wang, L., Lu, S., 2023. Adsorption of multicomponent VOCs on various biomass-derived hierarchical porous carbon: a study on adsorption mechanism and competitive effect. Chemosphere 313, 137513. https://doi.org/10.1016/j.chemosphere.2022.137513.

Jia, L., Shi, J., Long, C., Lian, F., Xing, B., 2020. VOCs adsorption on activated carbon with initial water vapor contents: adsorption mechanism and modified characteristic curves. Sci. Total Environ. 731, 139184. https://doi.org/10.1016/j.scitotenv.2020.139184.

Kaikiti, K., Stylianou, M., Agapiou, A., 2021. Use of biochar for the sorption of volatile organic compounds (VOCs) emitted from cattle manure. Environ. Sci. Pollut. Res. 28, 59141–59149. https://doi.org/10.1007/s11356-020-09545-y.

Kamali, M., Appels, L., Kwon, E.E., Aminabhavi, T.M., Dewil, R., 2021. Biochar in water and wastewater treatment - a sustainability assessment. Chem. Eng. J. 420, 129946. https://doi.org/10.1016/j.cej.2021.129946.

Klasson, K.T., Wartelle, L.H., Lima, I.M., Marshall, W.E., Akin, D.E., 2009. Activated carbons from flax shive and cotton gin waste as environmental adsorbents for the chlorinated hydrocarbon trichloroethylene. Bioresour. Technol. 100, 5045–5050. https://doi.org/10.1016/j.biortech.2009.02.068.

Kumar, A., Bhattacharya, T., 2021. Biochar: a sustainable solution. Environ. Dev. Sustain. 23, 6642–6680. https://doi.org/10.1007/s10668-020-00970-0.

Kumar, A., Singh, E., Khapre, A., Bordoloi, N., Kumar, S., 2020. Sorption of volatile organic compounds on non-activated biochar. Bioresour. Technol. 297, 122469. https://doi.org/10.1016/j.biortech.2019.122469.

Li, X., Zhang, L., Yang, Z., Wang, P., Yan, Y., Ran, J., 2020. Adsorption materials for volatile organic compounds (VOCs) and the key factors for VOCs adsorption process: a review. Sep. Purif. Technol. 235, 116213. https://doi.org/10.1016/j.seppur.2019.116213.

Li, J., Ma, X., Wu, H., Yang, L., 2021a. Adsorption of low-concentration VOCs on modified activated carbons in a humid atmosphere. Energy Fuels 35, 5090–5100. https://doi.org/10.1021/acs.energyfuels.0c03971.

Li, Z., Li, Y., Zhu, J., 2021b. Straw-based activated carbon: optimization of the preparation procedure and performance of volatile organic compounds adsorption. Materials 14, 3284. https://doi.org/10.3390/ma14123284.

Li, Y., Gupta, R., Zhang, Q., You, S., 2023. Review of biochar production via crop residue pyrolysis: development and perspectives. Bioresour. Technol. 369, 128423. https://doi.org/10.1016/j.biortech.2022.128423.

Lu, Y., Wang, H., Lu, Y.-Y., Ren, Z.-Q., Gao, N., Wang, J.-J., Huang, B.-C., Jin, R.-C., 2025. In-situ synthesis of lanthanum-coated sludge biochar for advanced phosphorus adsorption. J. Environ. Manag. 373, 123607. https://doi.org/10.1016/j.jenvman.2024.123607.

Lyu, H., Hu, K., Wu, Z., Shen, B., Tang, J., 2023. Functional materials contributing to the removal of chlorinated hydrocarbons from soil and groundwater: classification and intrinsic chemical-biological removal mechanisms. Sci. Total Environ. 879, 163011. https://doi.org/10.1016/j.scitotenv.2023.163011.

Ma, J., McHugh, T., Beckley, L., Lahvis, M., DeVaull, G., Jiang, L., 2020. Vapor intrusion investigations and decision-making: a critical review. Environ. Sci. Technol. 54, 7050–7069. https://doi.org/10.1021/acs.est.0c00225.

Mahmoodlu, M.G., Hassanizadeh, S.M., Hartog, N., Raoof, A., Van Genuchten, M.Th, 2015. Evaluation of a horizontal permeable reactive barrier for preventing upward diffusion of volatile organic compounds through the unsaturated zone. J. Environ. Manag. 163, 204–213. https://doi.org/10.1016/j.jenvman.2015.08.025.

Makoś-Chełstowska, P., Słupek, E., Gębicki, J., 2024. Agri-food waste biosorbents for volatile organic compounds removal from air and industrial gases – a review. Sci. Total Environ. 945, 173910. https://doi.org/10.1016/j.scitotenv.2024.173910.

Manap, N.R.A., Shamsudin, R., Maghpor, M.N., Hamid, M.A.A., Jalar, A., 2018. Adsorption isotherm and kinetic study of gas-solid system of formaldehyde on oil palm mesocarp bio-char: pyrolysis effect. J. Environ. Chem. Eng. 6, 970–983. https://doi.org/10.1016/j.jece.2017.12.067.

Mašek, O., Buss, W., Sohi, S., 2018. Standard biochar materials. Environ. Sci. Technol. 52, 9543–9544. https://doi.org/10.1021/acs.est.8b04053.

Masud, M.A.A., Shin, W.S., Sarker, A., Septian, A., Das, K., Deepo, D.M., Iqbal, M.A., Islam, A.R.M.T., Malafaia, G., 2023. A critical review of sustainable application of biochar for green remediation: research uncertainty and future directions. Sci. Total Environ. 904, 166813. https://doi.org/10.1016/j.scitotenv.2023.166813.

Millington, R.J., Quirk, J.P., 1961. Permeability of porous solids. Trans. Faraday Soc. 57, 1200. https://doi.org/10.1039/tf9615701200.

Nair, R.R., Mondal, M.M., Weichgrebe, D., 2022. Biochar from co-pyrolysis of urban organic wastes—investigation of carbon sink potential using ATR-FTIR and TGA. Biomass Convers. Biorefinery 12, 4729–4743. https://doi.org/10.1007/s13399-020-01000-9.

Nikam, S., Mandal, D., 2020. Experimental study of the effect of different parameters on the adsorption and desorption of trichloroethylene vapor on activated carbon particles. ACS Omega 5, 28080–28087. https://doi.org/10.1021/acsomega.0c03648.

Pochampally, S.V., Krishnaswamy, P., Obra, C., Mortazavian, S., Marti, E., Moon, J., 2023. Adsorption of chlorinated hydrocarbons onto non-activated biochars: biochar physicochemical characteristics and governing factors. Bioresour. Technol. Rep. 22, 101465. https://doi.org/10.1016/j.biteb.2023.101465.

Qiu, M., Liu, L., Ling, Q., Cai, Y., Yu, S., Wang, S., Fu, D., Hu, B., Wang, X., 2022. Biochar for the removal of contaminants from soil and water: a review. Biochar 4, 19. https://doi.org/10.1007/s42773-022-00146-1.

Rajabi, H., Hadi Mosleh, M., Prakoso, T., Ghaemi, N., Mandal, P., Lea-Langton, A., Sedighi, M., 2021. Competitive adsorption of multicomponent volatile organic compounds on biochar. Chemosphere 283, 131288. https://doi.org/10.1016/j.chemosphere.2021.131288.

Ribeiro, P.B., De Freitas, V.O., Machry, K., Muniz, A.R.C., Da Rosa, G.S., 2019. Evaluation of the potential of coal fly ash produced by gasification as hexavalent chromium adsorbent. Environ. Sci. Pollut. Res. 26, 28603–28613. https://doi.org/10.1007/s11356-018-3852-7.

Rossi, M.M., Silvani, L., Amanat, N., Petrangeli Papini, M., 2021. Biochar from pine wood, rice husks and iron-eupatorium shrubs for remediation applications: surface characterization and experimental tests for trichloroethylene removal. Materials 14, 1776. https://doi.org/10.3390/ma14071776.

Sadasivam, B.Y., Reddy, K.R., 2015a. Adsorption and transport of methane in biochars derived from waste wood. Waste Manag. 43, 218–229. https://doi.org/10.1016/j.wasman.2015.04.025.

Sadasivam, B.Y., Reddy, K.R., 2015b. Adsorption and transport of methane in landfill cover soil amended with waste-wood biochars. J. Environ. Manag. 158, 11–23. https://doi.org/10.1016/j.jenvman.2015.04.032.

Sadegh, F., Sadegh, N., Wongniramaikul, W., Apiratikul, R., Choodum, A., 2024. Adsorption of volatile organic compounds on biochar: a review. Process Saf. Environ. Prot.

Scheutz, C., Kjeldsen, P., 2003. Capacity for biodegradation of CFCs and HCFCs in a methane oxidative counter-gradient laboratory system simulating landfill soil covers. Environ. Sci. Technol. 37, 5143–5149. https://doi.org/10.1021/es026464+.

Settimi, C., Zingaretti, D., Verginelli, I., Baciocchi, R., 2025. Sulfidated zero-valent iron bimetals for passive remediation of chlorinated vapors in the subsurface. Environ. Pollut., 126202. https://doi.org/10.1016/j.envpol.2025.126202.

Settimi, C., Zingaretti, D., Verginelli, I., Baciocchi, R., 2023. Degradation of trichloroethylene vapors by micrometric zero-valent Fe Cu and Fe Ni bimetals under partially saturated conditions. J. Contam. Hydrol. 257, 104204. https://doi.org/10.1016/j.jconhyd.2023.104204.

Shen, Y., 2023. Biomass-derived porous carbons for sorption of volatile organic compounds (VOCs). Fuel 336, 126801. https://doi.org/10.1016/j.fuel.2022.126801.

Shen, Z., Zhang, Yunhui, Jin, F., Alessi, D.S., Zhang, Yiyun, Wang, F., McMillan, O., Al-Tabbaa, A., 2018. Comparison of nickel adsorption on biochars produced from mixed softwood and Miscanthus straw. Environ. Sci. Pollut. Res. 25, 14626–14635. https://doi.org/10.1007/s11356-018-1674-2.

Song, Q., Kong, F., Liu, B.-F., Song, X., Ren, H.-Y., 2024. Biochar-based composites for removing chlorinated organic pollutants: applications, mechanisms, and perspectives. Environ. Sci. Ecotechnol. 21, 100420. https://doi.org/10.1016/j.ese.2024.100420.

Tan, X., Ma, X., Li, X., Li, Y., 2024. An adsorption model considering fictitious stress. Fractal Fract 9, 17. https://doi.org/10.3390/fractalfract9010017.

Trigo, C., Cox, L., Spokas, K., 2016. Influence of pyrolysis temperature and hardwood species on resulting biochar properties and their effect on azimsulfuron sorption as compared to other sorbents. Sci. Total Environ. 566–567, 1454–1464. https://doi.org/10.1016/j.scitotenv.2016.06.027.

U.S. EPA, 2024. Regional Screening Level (RSL) Chemical-specific Parameters Supporting Table. May 2024. https://www.epa.gov/risk/regional-screening-levels-rsls-generic-tables. accessed on September 2024.

U.S. EPA, 2007. Toxicity and exposure assessment for children's health. Trichloroethylene (TCE). TEACH Chemical Summary. https://archive.epa.gov/region5/teach/web/pdf/tce_summary.pdf. (Accessed 15 June 2024).

U.S. EPA, 2004. In Situ Thermal Treatment of Chlorinated Solvents: Fundamentals and Field Applications. https://www.epa.gov/remedytech/situ-thermal-treatment-chlorinated-solvents-fundamentals-and-field-applications. accessed on September 2024.

Van Genuchten, M.Th, 1981. Analytical solutions of the one-dimensional convective-dispersive solute transport equation. Agric. Water Manag. 9, 79–80. https://doi.org/10.1016/0378-3774(84)90020-9.

Verginelli, I., Yao, Y., 2021. A review of recent vapor intrusion modeling work. Groundw. Monit. Remediat. 41, 138–144. https://doi.org/10.1111/gwmr.12455.

Vikrant, K., Kim, K.-H., Peng, W., Ge, S., Sik Ok, Y., 2020. Adsorption performance of standard biochar materials against volatile organic compounds in air: a case study using benzene and methyl ethyl ketone. Chem. Eng. J. 387, 123943. https://doi.org/10.1016/j.cej.2019.123943.

Wang, S., Song, L., He, H., Zhang, W., 2024. Volatile organic compounds (VOCs) in soil: transport mechanisms, monitoring, and removal by biochar-modified capping layer. Coatings 14, 270. https://doi.org/10.3390/coatings14030270.

Wei, Z., Seo, Y., 2010. Trichloroethylene (TCE) adsorption using sustainable organic mulch. J. Hazard. Mater. 181, 147–153. https://doi.org/10.1016/j.jhazmat.2010.04.109.

Xiang, W., Zhang, X., Chen, K., Fang, J., He, F., Hu, X., Tsang, D.C.W., Ok, Y.S., Gao, B., 2020. Enhanced adsorption performance and governing mechanisms of ball-milled biochar for the removal of volatile organic compounds (VOCs). Chem. Eng. J. 385, 123842. https://doi.org/10.1016/j.cej.2019.123842.

Yang, C., Miao, G., Pi, Y., Xia, Q., Wu, J., Li, Z., Xiao, J., 2019. Abatement of various types of VOCs by adsorption/catalytic oxidation: a review. Chem. Eng. J. 370, 1128–1153. https://doi.org/10.1016/j.cej.2019.03.232.

Yao, Y., Shen, R., Pennell, K.G., Suuberg, E.M., 2013. A review of vapor intrusion models. Environ. Sci. Technol. 47, 2457–2470. https://doi.org/10.1021/es302714g.

Yuan, P., Wang, J., Pan, Y., Shen, B., Wu, C., 2019. Review of biochar for the management of contaminated soil: preparation, application and prospect. Sci. Total Environ. 659, 473–490. https://doi.org/10.1016/j.scitotenv.2018.12.400.

Zhang, X., Gao, B., Creamer, A.E., Cao, C., Li, Y., 2017a. Adsorption of VOCs onto engineered carbon materials: a review. J. Hazard. Mater. 338, 102–123. https://doi.org/10.1016/j.jhazmat.2017.05.013.

Zhang, X., Gao, B., Zheng, Y., Hu, X., Creamer, A.E., Annable, M.D., Li, Y., 2017b. Biochar for volatile organic compound (VOC) removal: sorption performance and governing mechanisms. Bioresour. Technol. 245, 606–614. https://doi.org/10.1016/j.biortech.2017.09.025.

Zhao, Z., Wang, B., Theng, B.K.G., Lee, X., Zhang, X., Chen, M., Xu, P., 2022. Removal performance, mechanisms, and influencing factors of biochar for air pollutants: a critical review. Biochar 4, 30. https://doi.org/10.1007/s42773-022-00156-z.

Zhu, L., Shen, D., Luo, K.H., 2020. A critical review on VOCs adsorption by different porous materials: species, mechanisms and modification methods. J. Hazard. Mater. 389, 122102. https://doi.org/10.1016/j.jhazmat.2020.122102.

Zingaretti, D., Verginelli, I., Baciocchi, R., 2019. Dehalogenation of trichloroethylene vapors by partially saturated zero-valent iron. Sci. Total Environ. 647, 682–689. https://doi.org/10.1016/j.scitotenv.2018.08.011.

Zingaretti, D., Verginelli, I., Luisetto, I., Baciocchi, R., 2020. Horizontal permeable reactive barriers with zero-valent iron for preventing upward diffusion of chlorinated solvent vapors in the unsaturated zone. J. Contam. Hydrol. 234, 103687. https://doi.org/10.1016/j.jconhyd.2020.103687.